Available online at www.sciencedirect.com
SCIENCE DIRECT®
Nuclear Instruments and Methods in Physics Research A 538 (2005) 738–746
NUCLEAR INSTRUMENTS & METHODS IN PHYSICS RESEARCH Section A
www.elsevier.com/locate/nima

Differential absorption imaging for elemental analysis of thin samples using a soft laser-plasma X-ray source

S. Laville[a], L.A. Gizzi[a,1], P. Köster[a,2], L. Labate[a,*,1]

[a]*Intense Laser Irradiation Laboratory—IPCF (CNR), Via Moruzzi 1, 56124 Pisa, Italy*

Received 10 August 2004; accepted 6 September 2004
Available online 1 October 2004

Abstract

The differential X-ray imaging technique is a powerful tool for the detection of small concentrations of contrast agents in samples, as demonstrated recently by many biological and medical applications using synchrotron radiation. In this paper, we present an implementation of this technique using a laser-plasma soft X-ray source combined with an X-ray imaging system based upon a spherically bent Bragg crystal. Using a test sample containing a solution of LiBr of known concentration, we demonstrate that the use of our table-top configuration is suitable to detect Br inside our sample via differential imaging at the L_2 edge of Br at 7.7684 Å.

1. Introduction

The detection of specific elements or compounds in a sample is of particular interest in a wide range of fundamental and applied research fields. In some circumstances, information about the total concentration as well as the spatial distribution of a given element in a sample can be obtained by exploiting the self-emission properties of a specific radioactive tracing element included in the compound [1,2]. Alternatively, highly X-ray absorbing contrast agents are also used in combination with radiographic imaging techniques that provide a two-dimensional mapping of the X-ray absorption in the sample [3]. Techniques based upon these principles are currently used as clinical diagnostic techniques. The differential absorption imaging technique [4] is an alternative tool for accomplishing this task that only relies on the spectral properties of absorption of X-ray radiation by an atomic element. This technique is potentially suitable for the detection of small concentrations of contrast agents in biological samples. It is mainly based on the different photon mass absorption coefficient across one of the absorption edges of the chosen contrast agent injected in the

*Corresponding author. Tel.: +39 050 315 2255; fax: +39 050 315 2230.
E-mail address: luca.labate@ipcf.cnr.it (L. Labate).
[1]Also at INFN, Sezione di Pisa, Italy.
[2]Also at Dip. Fisica, Università di Pisa, Italy.

0168-9002/$ - see front matter © 2004 Elsevier B.V. All rights reserved.
doi:10.1016/j.nima.2004.09.004

sample of interest. Acquisition of two X-ray images of the sample with photon energies just below and above the edge allows a mapping of this sample to be obtained by simply performing the logarithmic subtraction of these two images. This procedure assumes that the two photon energies are so close to each other that all the other elements present in the sample do not exhibit notable contribution to the variation of the optical depth when changing photon energy. This basically assumes that such elements do not have absorption edges in the range of energy considered. The principle behind this technique has already been proposed for the detection of small concentrations of contrast agents for biological and medical applications. For instance, it is currently under study for imaging of coronary arteries in order to detect cardiovascular anomalies. For this method, known as coronary angiography [2,5–7], the contrast agent usually used is iodine. Such studies have already been carried out using monochromatic radiation emitted by different kinds of X-ray sources, such as synchrotron [2,3] or conventional X-ray tubes [6,8]. Although synchrotron is presently the most performing source in terms of brightness, the cost and the size of this facility limit its use to large-scale research centers rather than hospitals. On the other hand, X-ray tubes are not a good alternative, due to the impossibility of obtaining, at the same time, an X-ray beam with sufficient flux and a reasonable monochromaticity. More recently, laser–plasma Kα sources have also been suggested as possible compact sources for this kind of application [4,7,9]since they are typically table-top and exhibit quite intense X-ray pulses. From this kind of source, it is, therefore, possible to obtain quasi-monochromatic X-rays using the dispersion properties of a spherically bent crystal as it was recently proposed by Pikuz et al. [10].

In this paper, we present an investigation aimed at scaling the application of the differential absorption technique from the hard X-rays typically used for coronary angiography to the soft X-ray range, in order to carry out a quantitative elemental analysis of thin samples. Indeed, in order to visualize a sample using X-rays, the attenuation length of the radiation must be of the order of the thickness of the sample. For thin samples, say a few tens of microns, and in particular for biological samples, this condition is usually fulfilled in the soft X-ray range. Typically, we considered here photon energies ranging from 1 to 4 keV, which is well below the typical energies used for medical diagnostic applications (for instance, a few tens of keV for mammography [2]). In particular, we investigate the possibility of using a table-top laser-plasma soft X-ray source, combined with the diffractive crystal properties, for the development of a standard arrangement for a dedicated small-scale equipment for two-dimensional (2D) elemental mapping. In the experiment described here we used a test sample containing a solution of LiBr of known concentration. Differential imaging was performed using the L_2 edge of Br at 7.7684 Å (1596 eV). Imaging below and above this energy was carried out using two X-ray lines emitted from plasmas produced by an Al target.

A short basic introduction to the technique of differential absorption is first given. We then recall the basic features relative to the X-ray optical configuration used to obtain monochromatic X-rays. This is followed by the description of the experimental setup based on the laser-plasma X-ray source developed at the Intense Laser Irradiation Laboratory. We perform preliminary imaging of a test object consisting of a Fresnel zone-plate to discuss the spatial resolution achievable with our imaging system. Therefore, we show the experimental results obtained by applying the differential imaging to a thin sample containing the LiBr solution.

2. Principle of the differential imaging technique

In principle, the detection of a given element characterized by an absorption edge at a given wavelength, denoted by λ_{edge}, requires two images of the sample to be taken using monochromatic radiation at two different photon wavelengths, one (λ_1) just below the edge wavelength, and another one (λ_2) just above the edge. Under certain conditions, the logarithmic subtraction of these two images gives then directly a 2-D map of the

tracing element inside the sample (more details about the technique can be found elsewhere [2,4,6,7]). More quantitatively, the 2-D map of the intensity of the X-ray radiation transmitted by a sample irradiated at a normal incidence at a given photon wavelength can be written as

$$I^{(j)}(x,y) = I_0^{(j)}(x,y)\exp\left(-\sum_i \mu_i^{(j)}\int_s \rho_i(x,y,z)\,\mathrm{d}z\right), \quad (1)$$

where z is the coordinate along the direction of the incident beam, x and y are the coordinates perpendicular to z, $I_0^{(j)}(x,y)$ is the incident beam intensity, with the index $j=1,2$ identifying the two wavelengths, respectively, above and below the absorption edge, $\mu_i^{(j)}$ is the mass absorption coefficient of the ith element in the sample at the jth value of the wavelength, $\rho_i(x,y,z)$ is its density distribution and finally s is the thickness of the sample. Performing the logarithmic subtraction of the two distributions of intensity taken at the two photon wavelengths yields a map of the difference of optical depth

$$\Delta t(x,y) = \ln R(x,y) = \sum_i \Delta\mu_i \int_s \rho_i(x,y,z)\,\mathrm{d}z, \quad (2)$$

where $R(x,y) = I^{(2)}(x,y)I_0^{(1)}(x,y)/I_0^{(2)}(x,y)I^{(1)}(x,y)$ and $\Delta\mu_i = \mu_i^{(1)} - \mu_i^{(2)}$ is the difference of the mass absorption coefficient of the element at the two wavelengths.

We now restrict our analysis to the case in which the two values of the photon wavelength are close enough to neglect the variation of the optical depth of the other elements present in the substrate. This is generally justified provided these elements do not exhibit an absorption edge in the wavelength range considered. This assumption sets a limit to the minimum detectable surface density of the tracing element for a given surface density of substrate elements. In this case, the surface mass density σ_t of the tracing element can be written as

$$\sigma_t(x,y) = \int_s \rho_t(x,y,z)\,\mathrm{d}z = \frac{\ln R(x,y)}{\Delta\mu_t}. \quad (3)$$

The uncertainty on the detectable surface mass density of the tracing element is obtained from Eq. (3), considering the uncertainties on $\Delta\mu$ and R, and can be written as

$$\delta\sigma_t = \sqrt{\left(\frac{\delta(\Delta\mu_t)}{(\Delta\mu_t)^2}\ln R\right)^2 + \left(\frac{\delta R}{R\Delta\mu_t}\right)^2}. \quad (4)$$

From an experimental point of view, it comes out that, since tabulated values of μ are typically very accurate, the uncertainty on $\Delta\mu_t$ is negligible in comparison with the uncertainty on the measured intensities, considering that, in our experimental configuration, the wavelengths can be tuned experimentally very precisely by turning the crystal. Therefore, the uncertainty on the measurement of the surface mass density of a tracing element becomes

$$\delta\sigma_t = \frac{\delta R}{R\Delta\mu_t}. \quad (5)$$

This corresponds also to the minimum detectable surface mass density, which will be denoted as $\sigma_{\min}$, corresponding to the condition of a 100% relative error on the surface density ($\delta\sigma_t/\sigma_t = 1$).

3. Description of the monochromatic imaging system

The use of the differential imaging technique requires that the sample of interest is irradiated with monochromatic X-ray beams for which the wavelength can be tuned around the selected absorption edge of the contrast agent. In this work, we used the soft X-ray emission from highly ionized laser–produced plasmas. A detailed description of laser–plasma X-ray sources and their applicability to monochromatic imaging can be found elsewhere [11–13]. Here we only point out that since laser–plasmas are point-like X-ray sources characterized by a broad-band emission, an additional device is necessary for selecting the appropriate spectral component. In this case, the use of a spherically bent crystal allows spectral selection (monochromatization), beam focusing and imaging to be obtained simultaneously.

The main properties of an optical configuration based on a spherically bent crystal can be explained by considering two independent perpendicular planes, as indicated in Fig. 1. The first one,

known as the horizontal plane, is generally defined by the plane of incidence of the ray emitted by the source (denoted by S) impinging at the center of the crystal (O). The second one, passing through O, is perpendicular to the first one and is consequently named the vertical plane (in the literature, these planes are sometimes referred respectively, as the dispersive and the focusing planes). Due to the astigmatism of the optical configuration, after being reflected by the crystal, a beam is focused in the horizontal and vertical planes in different points called, respectively, the horizontal (denoted in what follows as F_H) and vertical (F_V) foci. For a given position of the source with respect to the crystal, the positions of the horizontal (b_H) and vertical (b_V) foci are given, respectively, by the following [10,14–16]:

$$\frac{1}{a}+\frac{1}{b_{H,V}}=\frac{1}{f_{H,V}}, \tag{6}$$

where a is the distance between the source (S) and the center of the crystal (O), $f_H=(R/2)\sin\vartheta_0$ is the horizontal focal distance and $f_V=R/(2\sin\vartheta_0)$ is the vertical focal distance. In these expressions, R is the radius of curvature of the crystal and ϑ_0 is the angle of incidence of the X-ray beam at the center of the crystal.

By placing an object between the source and the crystal a projection image of this object can be obtained in a plane after the crystal (see Fig. 1). When an angle of incidence ϑ_0 significantly different from $\pi/2$ is used, this configuration is astigmatic, and so the linear magnifications in the two planes are generally not the same and are given by [10,16]

$$M_H=\frac{a(q-b_H)}{b_H(a-p)}, \tag{7}$$

$$M_V=\frac{a(b_V-q)}{b_V(a-p)}, \tag{8}$$

where p is the distance from the object to the center of the crystal, M_H and M_V are, respectively, the horizontal and the vertical magnification and q is the distance between the center of the crystal and the detector. Due to the astigmatism, there is only one position of the detector plane where an undistorted image of the object can be observed. In this position both the horizontal and vertical magnifications are equal ($M_H=M_V$, denoted by M) and the image preserves the same aspect ratio as the object. It can be easily shown that this condition is only obtained when the detector is placed beyond F_H at a distance q from the center of the crystal given by

$$q=\frac{2b_Hb_V}{b_H+b_V}. \tag{9}$$

This indicates that the position of the detector does not depend on the position of the object between the source and the center of the crystal. The corresponding magnification is given by

$$M(p)=\frac{a-p_0}{a-p}, \tag{10}$$

where $p_0=2ab_H/(b_H+b_V)$ is obtained for a unit magnification. Images with a different magnification are then simply obtained by moving the object between the source and the center of the crystal (which means varying the distance p) and keeping the crystal and the detector fixed. When $p<p_0$, we have $M<1$, while $M>1$ if $p>p_0$.

However, in order to perform differential imaging which requires monochromatic X-rays, we need to use a particular configuration of this optical scheme, as it was recently proposed by Pikuz et al. [10,16]. This configuration, known as shadow monochromatic backlighting (SMB), requires that the source (S) is located on the Rowland circle, i.e., on the circle of diameter equal to the radius of curvature of the crystal and passing by its center of curvature. In this condition, it follows from Eq. (6) that $b_H=a=R\sin\vartheta_0$, which means that F_H is located on the Rowland circle like the source S, and the position of F_V is given by $b_V=R\sin\vartheta_0/(2\sin^2\vartheta_0-1)$. As discussed previously, the object to be imaged out is then placed at the distance p from the source. From Eqs. (9) and (10), it can be shown that in the SMB scheme, the image obtained is undistorted when $q=R/\sin\vartheta_0$ and that the corresponding magnification is then given by

$$M=\frac{1}{\tan^2\vartheta_0}\frac{1}{1-p/a}.$$

This shows that for a given angle of incidence ϑ_0 at the center of the crystal, in order to modify the magnification it is only necessary to change the

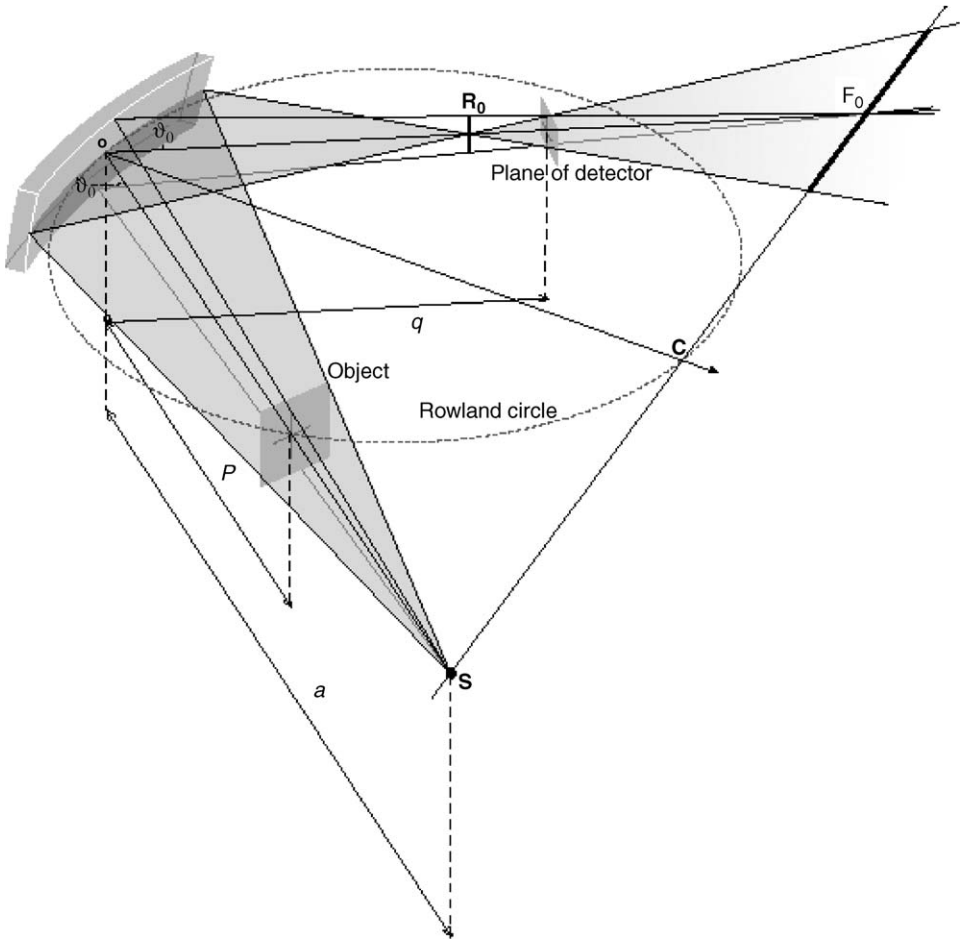

Fig. 1. Optical scheme of the configuration allowing a radiography of a thin sample to be obtained. The imaging X-ray beam is nearly monochromatic when the source is located on the Rowland circle.

position of the object between the source and the crystal by varying p.

It is important to point out that this configuration allows, theoretically, to obtain a good spatial resolution of the order of some μm over a field of view of some mm^2 [16], which is important for us to discriminate the region where the contrast agent is present or not when using the differential imaging technique.

4. Experimental setup

In this article we describe an experiment in which we used the SMB scheme to perform a radiography of a test sample to evaluate the imaging properties of the optical configuration. We also used another sample containing a known concentration of contrast agent to perform differential imaging using the monochromatic X-rays Bragg-reflected by the crystal. The experiment described here was carried out at the Intense Laser Irradiation Laboratory (ILIL) of the CNR in Pisa (Italy) using the PLX laser–plasma X-ray source [12,17] and the configuration is discussed in Section 3 and shown in Fig. 1. The X-ray radiation emitted by the source is collected using a spherically bent crystal positioned in such a way that the X-ray source is located on the Rowland circle. As discussed previously (see section 3), the

crystal then acts as a monochromator and consequently a highly monochromatic (the energy spread is of about 40 mÅ at 7.75 Å) X-ray beam is reflected on the detector. In our experiments, the X-ray emitting plasma was created by focusing a 7 ns, Nd:YAG laser pulse (with an energy of about 500 mJ) onto the surface of a cylindrical aluminum target. The laser wavelength was 1064 nm while the repetition rate of the laser system was 10 Hz. The focal spot diameter was measured to be about 20 μm, which leads to an intensity on the target of about 10^{13} W/cm^2. The 48×12 mm^2, spherically bent crystal (Mica, $2d = 19.9$ Å) had a radius of curvature $R = 150$ mm and was used in the second order of diffraction. The detection of X-rays was carried out using Princeton Instruments, high-dynamic range, cooled CCD equipped with a SiTE back-illuminated chip consisting of 1100×330 pixels, each of 24×24 μm^2 and is described in detail in [18]. Finally, the crystal was placed on a remote controlled mount to perform rotation on the Rowland circle which enabled the diffracted X-ray wavelength to be tuned.

5. Results and discussion

We present here the experimental results obtained concerning the implementation of this system for differential absorption micro-imaging. A comprehensive ray-tracing model of this crystal imaging system can be found elsewhere [14,19].

In our experiment, we performed differential imaging using a sample containing a contrast agent consisting of Br whose L_2 edge ($\Delta\mu_{Br} = 1506 \pm 10$ cm^2/g) is located at a wavelength of 7.7684 Å (1596 eV). K-shell emission from a laser-plasma source operating with an Al target is particularly suitable since it provides a number of spectral components around the Br L_2 edge. Indeed, the L_2 absorption edge of Br is located just between the $1s^2\,{}^1S-1s2p\,{}^1P$ He-α transition line from the He-like Al, located at a wavelength of 7.7571 Å (1598 eV) and a Li-like line at 7.875 Å (1574 eV). In our experiments, the spectral width of these two lines is essentially determined by the Doppler effect arising from the thermal motion of the emitting ions in the plasma. As a consequence, these lines exhibit a Gaussian shape. For an Al plasma at a temperature of the order of 100 eV, the relative width of an emitting line ($\Delta\lambda/\lambda$) is of the order of 10^{-4}. According to this estimate, the He-α and Li-like lines are sufficiently well-separated and monochromatic to be considered as good candidates for differential absorption measurements across the L_2 edge of Br.

Fig. 2a shows the beam pattern produced by the crystal tuned on the $1s^2\,{}^1S-1s2p\,{}^1P$ He-α line ($\lambda_0 = 7.7571$ Å) when no object is placed between the source and the crystal. According to the Bragg law $2d \sin \vartheta_0 = n\lambda_0$, where n is the order of diffraction (in our case $n = 2$), and the corresponding Bragg angle ϑ_0 at the center of the crystal is 0.894 rad. When the source is on the Rowland circle, using Eqs. (6), we find out that the position of the source is $a \simeq 11.7$ cm and the horizontal and vertical foci are, respectively, located at $b_H \simeq 11.7$ cm and $b_V \simeq 54.3$ cm.

Therefore, when a sample is placed between the source and the crystal, as shown in Fig. 1, a micrometer-resolution radiography of the sample at the selected photon wavelength (in our case, at the wavelength of the He-α line) is generated. From Eq. (9), it appears that an undistorted image of the sample is obtained when the detector is placed at a distance $q = 19.2$ cm from the center of the crystal. Fig. 2b shows a micro-imaging resolution test carried out on the system using an object consisting of a Fresnel zone-plate ($\lambda f = 0.116$ mm^2, radius of the first opaque zone roughly equal to 340 μm) whose total diameter is 7.5 mm. The Fresnel zone-plate was placed at a distance $p = 7$ cm from the center of the crystal which, according to Eq. (10), corresponds to a magnification $M \simeq 1.6$. An analysis of the image of Fig. 2b shows that in our experimental conditions, the spatial resolution in the horizontal direction is about 15 μm while in the vertical direction its value is about 50 μm. A comprehensive discussion on the spatial resolution properties of this imaging system can be found elsewhere [16,19]. Starting from this configuration, a small rotation of the crystal enables the beam photon wavelength at the center of the crystal to be set to a different value, while still keeping the sample onto the X-ray beams.

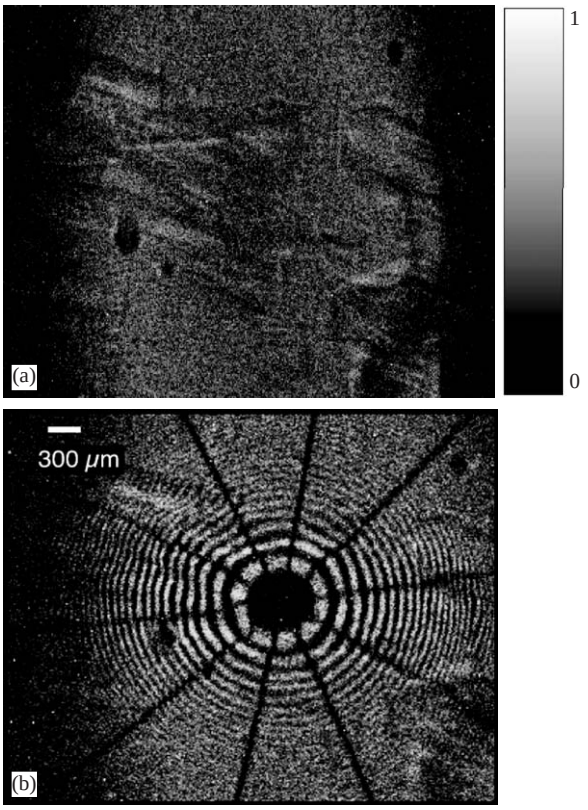

Fig. 2. (a) CCD image of the monochromatic X-ray beam as obtained with the experimental setup shown in Fig. 1. The crystal was tuned on the Al He-α line. (b) Monochromatic micro-imaging of a Fresnel zone plate ($\lambda f \simeq 0.116\,\mathrm{mm}^2$, total diameter 7.5 mm), used as a test sample.

A sample containing Bromine as a test element was prepared using a water solution of LiBr of a known concentration of 0.265 g/ml. An amount of 0.2 μl of the solution was deposited on the 30 μm thick paper substrate. The water was then removed in vacuum. The sample was mounted on a washer and placed between the source and the crystal as indicated in Fig. 1. A calculation based on the absorption properties of Br and on an average surface mass density of Br of $6 \times 10^{-4}\,(\pm 7 \times 10^{-5})\,\mathrm{g/cm}^2$ gives a corresponding optical depth difference of $\Delta t = 0.9 \pm 0.1$. The latter value will be compared with the measured one using the differential imaging technique.

Figs. 3a and b show X-ray images of the sample normalized to the incident intensity, i.e., the ratio between the X-ray beam transmitted through our sample and the incident one $(I^{(i)}(x,y)/I_0^{(i)}(x,y)$ for $i = 1, 2)$, at the two wavelengths below ($\lambda_1 = 7.75$ Å, next to the He-α line) and above ($\lambda_2 = 7.80$ Å, next to the Li-like line) the L_2 absorption edge of Br. The image on Fig. 3a was obtained accumulating X-ray flux over 10 X-ray pulses (i.e., 10 shots of the driving laser) at 10 Hz, while the image on Fig. 3b was obtained by integrating over 300 X-ray pulses. The images

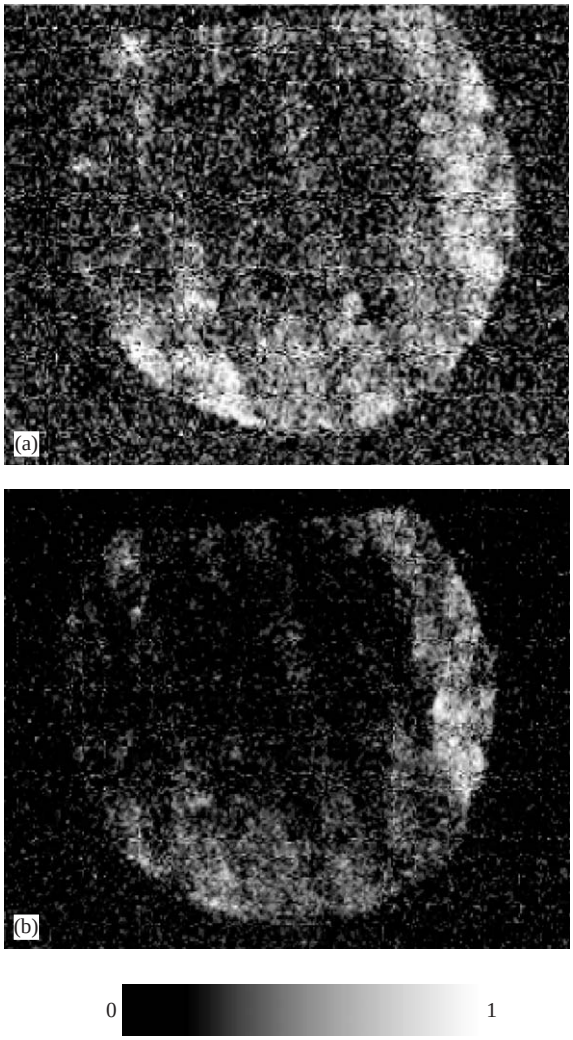

Fig. 3. Experimental X-ray beam transmitted through the LiBr sample used in our experiment. (a) The image is obtained at a wavelength $\lambda_a \simeq 7.87$ Å just above the Br L_2 absorption edge. (b) The image is taken at $\lambda_b \simeq 7.75$ Å, just below the edge.

consist of a circular region (inside the washer) with an inner, irregularly shaped darker (optically thicker) region due to the LiBr deposit. The parallel darker lines visible on the images are a consequence of the fiber-like structure of the paper substrate that results in modulations of the paper thickness, and consequently, modulations on the transmitted intensity. Finally, the shadow due to the washer used to hold the sample is also visible in the images.

A quantitative analysis of these results has been carried out using Eq. (2) and averaging the result on the area of the sample containing the LiBr deposit. The measurements give an average optical depth difference $\Delta t = 1.1 \pm 0.8$ that corresponds to a surface mass density $\sigma = 7.3 \times 10^{-4} (\pm 5 \times 10^{-4})\,\mathrm{g/cm^2}$. Such a value of optical depth difference is in agreement with the value of $\Delta t = 0.9 \pm 0.1$ expected from the presence of Br. The large uncertainty found in our measurements, compared with the uncertainty given by Eq. (5), is partly due to the single-photon noise arising from diffuse X-ray scattering, especially for the measurement at the photon energy above the edge, where too high absorption from Br occurs. In view of these considerations, higher signal-to-noise ratios should be obtained for samples with a lower surface density, as in the case of real tracing concentrations. In this case, the lower limit to the detectable surface density of Br is given by the instrumental uncertainty on the transmitted X-ray beam intensity due to the intensity resolution of the detector.

In the case of a 14-bits detector, we have $\delta I/I = 6.2 \times 10^{-4}$, which leads to $\delta R/R \simeq 2.5 \times 10^{-4}$. According to Eq. (5), it can be shown that these values give a minimum detectable surface mass density of $\sigma_{\min} \simeq 2 \times 10^{-7}\,\mathrm{g/cm^2}$. Assuming a sample thickness of 50 μm, a typical value of the X-ray attenuation length in the soft X-ray range for biological materials, we find that the minimum detectable average mass density is of the order of $\rho_{\min} \simeq 40\,\mu\mathrm{g/cm^3}$.

In some cases, the element searched for may not be uniformly distributed, as in the case of complex biological systems, where the tracing element can be found in well-localized (typically micrometer sized) regions with specific spatial properties (such as interstitial regions, vessels, capillaries, etc.). In these regions, the local concentration of the tracing element can be much higher than the average value. Consequently, provided sufficient spatial resolution is available in the imaging system, local concentrations of tracing elements can be detected even when average concentration values are well below the minimum detectable average value. Therefore, the value of the detectable average mass density derived above should only be regarded as an estimate by defect.

Another consideration concerns the other elements present in our sample with substantial abundances (mainly Li, C, H and O). All these elements exhibit a smooth change, but no absorption edges, of the mass absorption coefficient across the two wavelengths considered in our measurement. A simple calculation shows that the variation of optical depth of these elements across the edge of Br is also much lower that the one obtained for Br. Consequently, the change of optical depth expected for the presence of elements other than Br is reasonably negligible and Eq. (3) is a good approximation for the surface mass density of Br inside the sample.

6. Conclusions

In this paper, we have presented experimental results obtained for differential imaging of a sample containing Br using a laser-plasma soft X-ray source. Using a Fresnel zone-plate, we have shown that our soft X-ray source combined with a spherically bent crystal enables one to perform monochromatic imaging with spatial resolutions of the order of a few tens of microns. This resolution can be achieved on a sample a few millimeters in size. We have performed differential imaging of a thin sample containing a solution of Br. We were able to detect a significant change in the optical depth of the sample by changing the imaging X-ray wavelength by less than 0.1 Å. This enabled us to measure the surface density of Br in our test sample.

Important issues need to be addressed in order to make this method a general-purpose technique for the detection of trace-level elements in thin

samples. The main aspect concerns the possibility of extending the range of applicability to other absorption edge wavelengths, i.e., other elements. To this purpose, suitable emission photon energies close to the absorption edge under investigation and, consequently, a suitable target material must be identified. On the other hand, the possibility of using a laser-driven plasma source may result in an easy access to the technique on the basis of a small-scale dedicated laboratory. This could yield the possibility of improving the image quality and spatial resolution of widely used techniques like self-emission radiography, in these samples. In addition, the possibility of using non-radioactive tracing elements opens new possibilities for radioactive-free laboratory diagnostics in medicine and biology. Although the results presented here remain quite encouraging, the large uncertainty found in our measurements which is mainly due to the single-photon noise arising from diffuse X-ray scattering must be improved in order to provide a value of the concentration with higher accuracy. In addition, although the assumption of neglecting the change of optical depth due to the presence of elements other than Br is reasonable in our experimental conditions, the precision of the measurements can be improved using other wavelengths in order to eliminate the influence of elements other than the contrast agent. In view of all these considerations, higher signal-to-noise ratios should be obtained for samples with a much lower detectable surface density, as in the case of tracing concentrations commonly used in biological samples.

Acknowledgements

We would like to thank M. Galimberti, A. Giulietti, D. Giulietti and P. Tomassini for their scientific support and A. Barbini, A. Rossi, A. Salvetti, W. Baldeschi and M. Voliani for their invaluable technical assistance. SL acknowledges financial support from the European Research Training Network XPOSE Contract No. HPRN-CT-2000-00160. LL acknowledges financial support from MIUR (Project "Metodologie e diagnostiche per materiali ed ambiente"). This work was partially supported by the MIUR Project "Impianti innovativi multiscopo per la produzione di radiazione X".

References

[1] E. Barbarics, J.F. Kronauge, C.E. Costello, Gy.A. Jànokp, B.L. Holman, A. Davison, A.G. Jones, Nucl. Med. Biol. 21 (1994) 583.
[2] R. Lewis, Phys. Med. Biol. 42 (1997) 1213.
[3] P. Suortti, W. Thomlinson, Phys. Med. Biol. 48 (2003) R1.
[4] C. Tillman, I. Mercer, S. Svanberg, J. Opt. Soc. Am. B 13 (1996) 209.
[5] T. Dill, W.-R. Dix, C.W. Hamm, M. Jung, W. Kupper, M. Lohmann, B. Reime, R. Ventura, Eur. J. Phys. 19 (1998) 499.
[6] C.K. Gary, M.A. Piestrup, D.G. Boyers, C.I. Pincus, R.H. Pantell, G.B. Rothbart, Med. Phys. 20 (1993) 1527.
[7] E. Andersson, G. Hölzer, E. Förster, M. Grätz, L. Kiernan, A. Sjögren, S. Svanberg, J. Appl. Phys. 90 (2001) 3048.
[8] G. Baldazzi, D. Bollini, M. Gambaccini, M. Gombia, L. Ramello, A. Tuffanelli, Nucl. Instr. and Meth. B 213 (2004) 603.
[9] S. Svanberg, S. Andersson-Engels, R. Cubeddu, E. Förster, M. Grätz, K. Herrlin, G. Hölzer, L. Kiernan, C. Klinteberg, A. Persson, A. Pifferi, A. Sjögren, C.-G. Wahlström, Laser Part. Beams 18 (2000) 563.
[10] T.A. Pikuz, A.Ya. Faenov, M. Fraenkel, A. Zigler, F. Flora, S. Bollanti, P. Di Lazzaro, T. Letardi, A. Grilli, L. Palladino, G. Tomassetti, A. Reale, L. Reale, A. Scafati, T. Limongi, L. Alainelli, M. Sanchez del Rio, Laser Part. Beams 19 (2002) 285.
[11] D. Giulietti, L.A. Gizzi, Riv. Nuovo Cimento 21 (1998) 1.
[12] L.A. Gizzi, C.A. Cecchetti, M. Galimberti, D. Giulietti, A. Giulietti, P. Köster, L. Labate, S. Laville, P. Tomassini, Laser Part. Beams, accepted for publications.
[13] L. Labate, M. Galimberti, A. Giulietti, D. Giulietti, L.A. Gizzi, P. Tomassini, G. Di Cocco, Nucl. Instr. and Meth. A 495 (2002) 148.
[14] M. Sanchez del Rio, M. Fraenkel, A. Zigler, A.Ya. Faenov, T.A. Pikuz, Rev. Sci. Instrum. 70 (1999) 1614.
[15] F. Blasco, C. Stenz, F. Salin, A.Ya. Faenov, A.I. Magunov, T.A. Pikuz, I.Yu. Skobelev, Rev. Sci. Instrum. 72 (2001) 1956.
[16] M. Sanchez del Rio, L. Alianelli, T.A. Pikuz, A.Ya. Faenov, Rev. Sci. Instrum. 70 (2001) 3291.
[17] S. Marzi, A. Giulietti, D. Giulietti, L.A. Gizzi, A. Salvetti, Laser Part. Beams 18 (2000) 109.
[18] L. Labate, M. Galimberti, A. Giulietti, D. Giulietti, L.A. Gizzi, R. Numico, A. Salvetti, Laser Part. Beams 19 (2001) 117.
[19] L. Labate, M. Galimberti, A. Giulietti, D. Giulietti, L.A. Gizzi, P. Köster, S. Laville, P. Tomassini, Laser Part. Beams, accepted for publication.